Nuclear Science and Techniques (2025) 36:43
https://doi.org/10.1007/s41365-024-01617-9

Resonance analysis of ^{159}Tb(n, γ) reaction based on the CSNS Back-n experiment

De-Xin Wang[1,2] · Su-Ya-La-Tu Zhang[1,2] · Wei Jiang[3,4] · Jie Ren[5] · Mei-Rong Huang[1,2] · Jing-Yu Tang[6] · Xi-Chao Ruan[5] · Hong-Wei Wang[7] · Long-Xiang Liu[7] · Xue Li[1,2] · Dan-Dan Niu[1,8] · Guo Li[1,2] · Gu-Fu Meng[1,2] · Yong-Shun Huang[1,2] · Zhi-Long Wang[1,2] · Yu Bai[1,2] · Xue Yang[1,2]

Received: 16 April 2024 / Revised: 5 October 2024 / Accepted: 17 October 2024 / Published online: 28 January 2025

Abstract
The neutron capture resonance parameters for ^{159}Tb are crucial for validating nuclear models, nucleosynthesis during the neutron capture process, and nuclear technology applications. In this study, resonance analyses were performed for the neutron capture cross sections of ^{159}Tb measured at the China Spallation Neutron Source (CSNS) backscattering white neutron beamline (Back-n) facility. The resonance parameters were extracted from the *R*-Matrix code SAMMY and fitted to the experimental capture yield up to the 1.2 keV resolved resonance region (RRR). The average resonance parameters were determined by performing statistical analysis on the set of the resonance parameters in the RRR. These results were used to fit the measured average capture cross sections using the FITACS code in the unresolved resonance region from 2 keV to 1 MeV. The contributions of partial waves $l = 0, 1, 2$ to the average capture cross sections are reported.

Keywords Statistical analysis · Resonance parameters · ^{159}Tb(n,γ) cross section · γ

1 Introduction

Resonance parameters are nuclear data that play a crucial role in areas such as nuclear energy, security, and structure. These parameters are mainly obtained from neutron resonance spectroscopy and include the neutron strength function (S_0), average radiation width ($\langle\Gamma_\gamma\rangle$), and average level spacing (D_0) between the resonances [1]. These parameters are critical for substantiating nuclear structure models and serve as key inputs for nuclear physics applications, such as calculating Maxwellian-averaged cross sections (MACS) at keV energies that are relevant to nuclear astrophysics [2, 3].

In stellar nucleosynthesis, the neutron capture cross sections of rare-earth isotopes constitute a fundamental component of the slow neutron capture process (s-process)

This work was supported by the National Natural Science Foundation of China (Nos.12365018, U2032146, 12465024) and Natural Science Foundation of Inner Mongolia (Nos. 2023MS01005, 2024ZD23, 2024FX30), and the program of Innovative Research Team and Young Talents of Science and Technology in Universities of Inner Mongolia Autonomous Region (Nos. NMGIRT2217, NJYT23109).

✉ Su-Ya-La-Tu Zhang
zsylt0416@163.com

1 College of Physics and Electronics, and Institute of Nuclear Physics, Inner Mongolia Minzu University, Tongliao 028043, China

2 Inner Mongolia Joint Key Laboratory of Nuclear and Radiation Detection, Tongliao 028043, China

3 Chinese Academy of Sciences, Institute of High Energy Physics, Beijing 10049, China

4 Spallation Neutron Source Science Center, Dongguan 523803, China

5 Key Laboratory of Nuclear Data, China Institute of Atomic Energy, Beijing 102413, China

6 School of Nuclear Science and Technology, University of Science and Technology of China, Hefei 230026, China

7 Chinese Academy of Sciences, Shanghai Advanced Research Institute, Shanghai 201210, China

8 Center for Theoretical Physics, China Institute of Atomic Energy, Beijing 102413, China

and significantly influence the calculated stellar element abundances and astrophysical reaction rates [4]. For Terbium-159, a monoisotopic element, scarce neutron capture cross-sectional data are available from 1 eV to 1 MeV [5]. Additionally, the data presently accessible within this energy range are not only outdated, but also lack the requisite detail, leading to considerable inconsistencies in the resonance parameters. Previously reported experimental data shows that S_0 and D_0 vary from 0.9×10^{-4} to 1.56×10^{-4} and 3.21 to 4.40 eV [6–8]. Specifically, the latest evaluated nuclear data library, ENDF/B-VIII.0 [7], incorporates resonance parameters from an earlier database, JENDL−2.0, which utilized neutron capture measurements by Ohkubo et al. [9] and Mizumoto et al. [6] and data from Mughabghab [10]. Although their resonance parameters are nearly identical, JEFF−3.3 [11] and ENDF/B-VIII.0 [7] have different approaches to specific resonant structures and smooth regions.

In this study, the average resonance parameters were derived from the statistical analysis of the individual resonance parameters in the resolved resonance region (RRR) of the China Spallation Neutron Source (CSNS) backscattering white neutron beamline (Back-n) experimental neutron capture data. These results were used as input values for fitting the measured average capture cross sections with the FITACS code from 2 keV to 1 MeV. The average capture cross sections are given for partial waves $l = 0, 1, 2$ and are compared with the corresponding data from the literature and the evaluation nuclear data library.

In Sect. 2, the CSNS Back-n neutron capture cross-section experiments and resonance analysis results are outlined. Section 3 presents a statistical analysis of the resolved resonance region parameters. In Sect. 4, the results are integrated with FITACS to analyze the unresolved resonance region (URR). Finally, Sect. 5 summarizes the discussions and conclusions.

2 Neutron capture measurement

2.1 Back-n facility at CSNS

The measurements were conducted at the CSNS Back-n. The CSNS comprises an 80 MeV linear accelerator, a 1.6 GeV proton synchrotron (PS), two beam transport lines, a target station, three spectrometers, and the associated instrumentation [12, 13]. At the CSNS, spallation neutrons are generated by a 1.6 GeV/c proton beam with a 41 ns full width at half maximum from the PS incident on a tungsten target. The PS operates in either double- or single-beam cluster mode, delivering pulses at 25 Hz and an average current of 64 μA. A dedicated 15 ° deflection magnet designed by CSNS steers the proton beam before the target, separating the backscattered white neutron beam from the primary proton beam [14].

The Back-n beamline is situated 80 m downstream of the CSNS proton beam. It comprises two experimental stations: 55 m (ES#1) and 76 m (ES#2). ES#2 is outfitted with two different systems for capture experiments: the 4π GTAF-II array of 40 BaF_2 detectors for total absorption calorimetry and a total energy detector consisting of four low-sensitivity C_6D_6 detectors [15]. The neutron flux at the ES#2 sample position is $6.92 \times 10^5\ cm^{-2} \cdot s^{-1}$ over an energy range of 0.3 eV to 200 MeV distributed over three beam spot sizes: ($\Phi 20\,mm$, $\Phi 30\,mm$, and $\Phi 60\,mm$). The neutron spectrum was characterized using a Li-Si detector and a calibrated fission chamber, exploiting the standard ^{6}Li(n,t) and ^{235}U(n,f) reactions, respectively [16]. Additionally, a silicon flux monitor (SiMon) comprising a thin ^{6}LiF converter layer and eight silicon detectors positioned 20mm upstream of the sample continuously monitored the beam intensity [17–19].

2.2 The ^{159}Tb and samples

In this study, neutron capture cross-sectional measurements of ^{159}Tb were performed using a C_6D_6 detector array. A metallic sample of pure terbium with a diameter of 30.0mm and area density of 6.27×10^{-4} atom/barn was used for the prompt capture γ-ray measurement. A natural lead ^{nat}Pb with a diameter and thickness of 0.53mm was used to evaluate the in-beam γ-ray and neutron-induced background [13]. Additionally, ^{197}Au sample with thickness of 0.1mm was used to normalize the neutron capture data. An empty sample holder was placed on the beam to measure the background it generates. The evaluated background spectrum was normalized using the black resonance technique, which made it possible to distinguish between background and true signals. Samples ^{59}Co and ^{181}Ta were employed as neutron filters. Sample preparation was performed by the Department of Nuclear Physics of the China Institute of Atomic Energy. Much more details on the experimental setup can be found in Ref. [20–26].

2.3 Background deduction and data analysis

Background determination is a major challenge in experimental studies. The experimental data analysis was largely dependent on Monte Carlo simulations conducted using the Geant4 toolkit [27], which accurately reproduced the experimental configuration and formed a critical foundation for subsequent analyses. To maximize the precision of the measured gamma energy spectra, we implemented a rigorous efficiency correction that accounted for gamma energy in detection efficiency. This was achieved using the pulse-height weighting technique (PHWT) [28], which applies weighting functions to ensure that efficiency is independent of the cascade path and proportionality to the known cascade energy.

In addition to simulations, essential experimental measurements were performed using neutron filters composed of ^{59}Co and ^{181}Ta [20]. Here, we employed the black resonance technique to normalize the experimental background, enabling the separation of the background contributions from the true spectrum. This systematic approach is crucial for obtaining the required capture yield precision. The experimental neutron capture yield as a function of E_n is calculated as follows

$$Y_{exp}(E_n) = \frac{C^w(E_n) - C^b(E_n)}{f_{Au} \cdot \Phi(E_n) \times E_c}, \tag{1}$$

where $C^w(E_n)$ and $C^b(E_n)$ are the weighted count and total background spectra, respectively, f_{Au} is the normalization factor determined using the saturated resonance technique for the 4.9 eV resonance of the Au sample, $\Phi(E_n)$ is the neutron flux spectrum, and E_c is the detection efficiency of a capture event.

2.4 Resolved resonance region

This performs a theoretical reanalysis of ^{159}Tb neutron capture yield from a previous experiment [13] and interprets its statistical properties. We obtained the fundamental resonance parameters by fitting the measured ^{159}Tb(n,γ) capture yields in the resonance region using the R-matrix code SAMMY [29], based on the Reich-Moore approximation. The experimental conditions, neutron multiple scattering, self-shielding, and Doppler effects were included in the SAMMY code fitting. The resonance spin J and partial radiative and neutron widths Γ_n and Γ_γ, respectively, cannot be determined accurately using the capture measurement. Only the resonance energy and capture kernel k, which are directly related to the resonance area, can be reliably obtained from these capture measurements [30, 31]. The k defined as

$$k = g\frac{\Gamma_n\Gamma_\gamma}{\Gamma_n + \Gamma_\gamma}, \tag{2}$$

where g indicates the spin (statistical) weighting factor and Γ_n and Γ_γ are the partial neutron and radiative widths, respectively. Usually, g is given by

$$g = \frac{2J+1}{(2I+1)(2s+1)}, \tag{3}$$

where J is the compound nucleus resonance spin (total angular momentum) and I and s denote the target and neutron spins, respectively. In Fig. 1(a), the measured neutron capture yields at the resonance energy of 11.04 eV are fitted with the different spin J by the SAMMY code. Both $J = 1$ and $J = 2$ are well fitted to the experiment, as expected. The

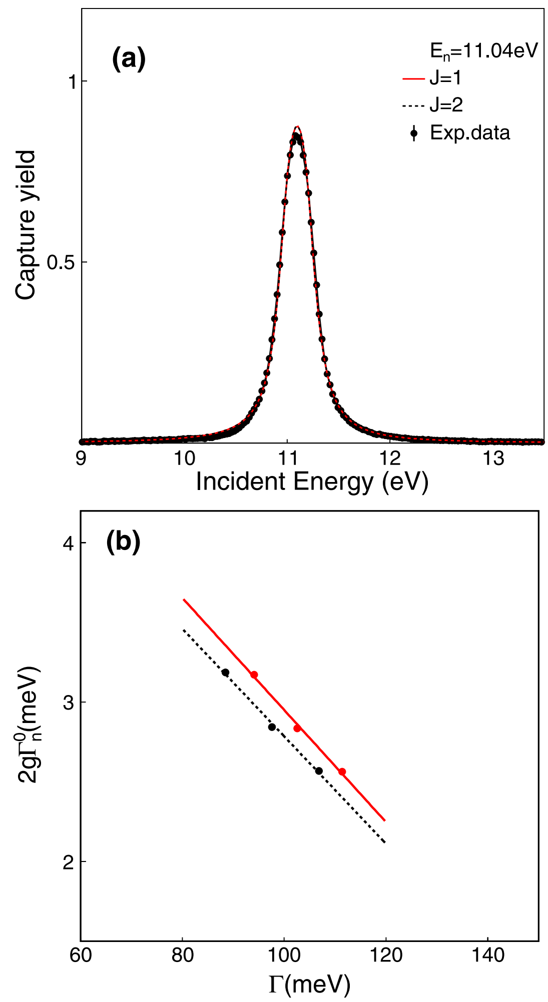

Fig. 1 (Color online) (a)The SAMMY fit to the measured yield at E_n =11.04 eV with different spins J. (b) Resonance parameters analysis in the $(\Gamma, 2g\Gamma_n^0)$ plane at 11.04 eV. The red solid line and black dashed line indicate $J = 1$ and $J = 2$, respectively

relationships between the resonance parameters are given in the $(\Gamma, 2g\Gamma_n^0)$ plane at E_n=11.04 eV resonance for different J, as shown in Fig. 1(b). The solid red and dashed black lines indicate $J = 1$ and $J = 2$, respectively. The two lines of Fig. 1(b) means there are many group of values in Γ_n and Γ_γ with fitted results for one of spin J (eg. $J = 1$ or $J = 2$). Usually, even when both the capture and transmission data are available, accurately establishing the spin factor remains challenging [9].

Experimental studies focused on calculating the resonance spins for ^{159}Tb are scarce. Among the available methods, transmission measurements using polarized neutrons on polarized ^{159}Tb nuclei have proven to be more precise in identifying the resonance J values. These measurements were reported in [32]. Given the scarcity of data and the high precision of this method, we adopted resonance spin values from [32] for our R-matrix analysis. Using this approach, we avoided some limitations of parameter extraction while relying on the most accurate spin information available.

We used SAMMY code for the resonance analysis of the ^{159}Tb neutron capture yield data from 1 eV to 1.2 keV [13]. Each SAMMY fitting iteration provided the initial resonance parameter values, which were iteratively refined until convergence. Below 100 eV, SAMMY was initialized with the parameter set from Table VII in Ref. [13]. Above 100 eV to 1.2 keV, initial parameters were taken from the JEFF–3.3 database [11]. Figure 2 compares the ^{159}Tb capture yield (black dots) with the SAMMY fit results (red lines). The resonance parameters are listed in Table 3.

3 Statistical properties of the resonance parameters

3.1 Average level spacing and average radiative width

The resonance distribution as a function of the neutron energy in the experimental measurements was directly related to the nuclear-level density ρ of the compound nuclei at the neutron separation energy. Specifically, ρ^J for a given spin J can be derived from the number of observed resonances N^J within the neutron energy interval ΔE_n using

$$\rho^J = \frac{N^J}{\Delta E_\mathrm{n}} = \frac{1}{\langle D^J \rangle}, \tag{4}$$

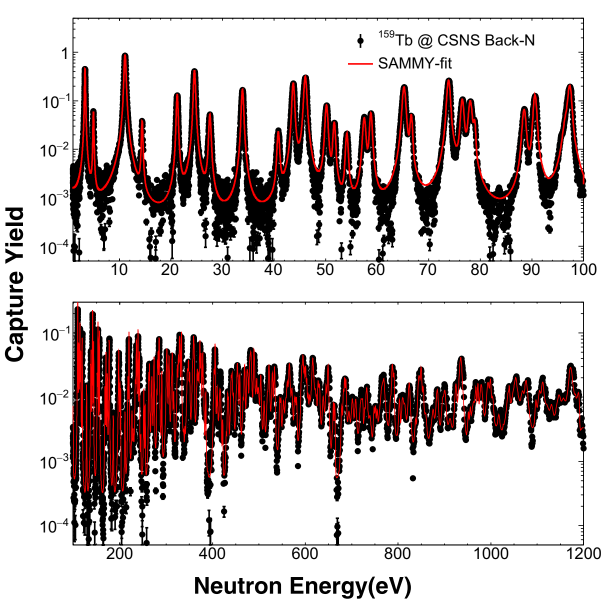

Fig. 2 (Color online) SAMMY fits of ^{159}Tb capture yield data from 1 eV to 1.2 keV

where D^J represents the average level spacing of spin J. The latter can be calculated based on the cumulative distribution of the observed resonances $N^J(E_\mathrm{n})$:

$$N^J(E_\mathrm{n}) = a + \langle D^J \rangle E_\mathrm{n}. \tag{5}$$

The spacing between successive resonances, which share the same total angular momentum and parity, was predicted to exhibit random behavior, which was verified experimentally. For a series of N consecutive resonances at energy E_i, the level spacing is defined as $D_i = E_i - E_{i-1}$. The probability distribution of these level spacings is expected to follow the Wigner-Dyson distribution [33] as Eq.(6).

$$p(x)\mathrm{d}x = \frac{\pi x}{2} e^{\left(-\frac{\pi x^2}{4}\right)} \mathrm{d}x, \quad x = \frac{D_i}{\langle D \rangle}. \tag{6}$$

The Wigner-Dyson law provides a mathematical prediction of the level spacing distribution in chaotic systems, accurately reproducing experimental observations. For narrow-spaced resonances, the level repulsion effect leads to a distribution that disappears at small spacings, reflecting the repulsive nature of close levels. The Wigner-Dyson distribution predicts an average spacing of $\langle x \rangle = 1$ and variance of $\sigma^2 = \left(\frac{4}{\pi} - 1\right)$. Consequently, the relative uncertainty in the average level spacing obtained from the N observed resonances can be expressed by Eq.(7):

$$\frac{\Delta D}{\langle D \rangle} = \sqrt{\frac{1}{N}\left(\frac{4}{\pi} - 1\right)}. \tag{7}$$

The cumulative number of experimentally observed levels as a function of neutron energy is shown in Fig. 3. The cumulative number of resonance analyses revealed differences between the data provided in Refs. [34] which is greater than 100 eV. Furthermore, when the neutron energy increased, the percentage of missed resonances increased progressively, a behavior that can be explained by statistical fluctuations. A linear fit was used to determine the average level spacing D_0, which was 3.84(4) electronvolt below 100 electronvolt. The consistency of the observed spin-experimental level spacing distribution was tested by comparing this value with the predicted theoretical Wigner-Dyson distribution.

The average radiative width $\langle \Gamma_\gamma \rangle$ was calculated exclusively within the energy range below 100 eV. Figure 4 shows the radiative width obtained by analyzing all resonances obtained from the SAMMY fits. The calculated weighted average of the entire energy spectrum was $\langle \Gamma_\gamma \rangle = 102.6(13)$ meV. Significant deviations of the individual values from the mean values were primarily attributed to the substantial correlations between the radiative and neutron widths. These divergences do not imply the non-statistical behavior of the radiative width because all resonances at higher energies can

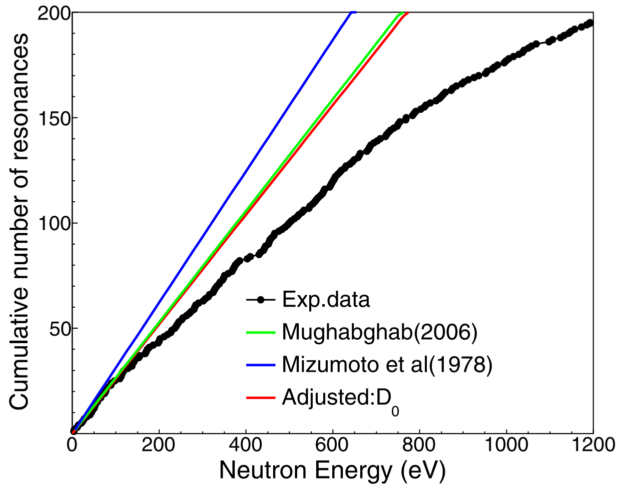

Fig. 3 (Color online) Cumulative number of levels as a function of neutron energy. The green line correspond to $D_0 = 3.78$ eV recommended by Mughabghab [10]. The blue line corresponds to $D_0 = 3.21$ eV, which was reported by Mizumoto et.al [6]. The red line corresponds to the adjusted fitting of currently accumulated experimental data below 100 eV, producing $D_0 = 3.84 \pm 0.04$ eV

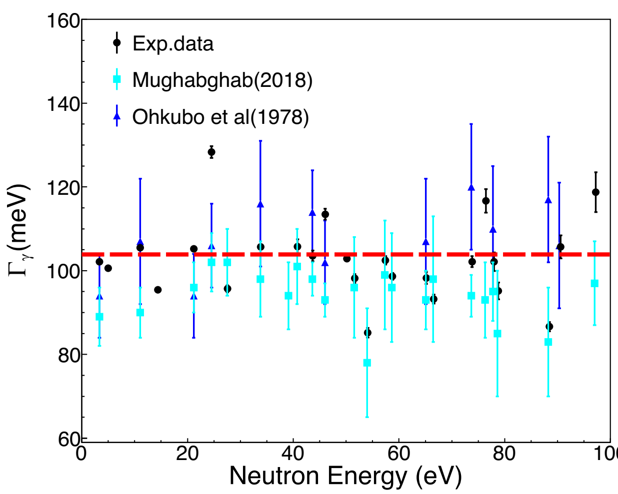

Fig. 4 (Color online) Fitted values for the radiative widths below 100 eV. The red-dashed line corresponds to the weighted average value $\langle\Gamma_\gamma\rangle = 102.6(13)$ meV

be satisfactorily analyzed with a fixed value corresponding to $\langle\Gamma_\gamma\rangle$.

3.2 Neutron width

The neutron width Γ_n of the neutron energy E_0 is correlated with the average lifetime τ_n relative to neutron emission decay. This relationship is given by an expression reported in [35]:

$$\Gamma_n = \hbar/\tau_n, \tag{8}$$

where $\hbar$ denotes the reduced Planck's constant. The width can be approximately considered as the time required for the excitation energy to be concentrated on a specific neutron and the probability that a neutron penetrates the nuclear potential barrier. Thus, the neutron width can be viewed as the probability per unit time that a compound nucleus emits neutrons. Therefore, the neutron width Γ_n is given by

$$\Gamma_n = \hbar p/t_0, \tag{9}$$

where t_0 is the average lifetime before the energy is concentrated on an individual neutron in a specific excited state and p is the actual potential barrier penetrability. However, the reduced neutron width Γ_n^0 at 1 eV for s-wave neutrons can be defined as

$$\Gamma_n^0 = \hbar p^0/t_0 = \Gamma_n/\sqrt{E_0}, \tag{10}$$

where p^0 is the number of 1 eV neutrons. Thus, insight into the properties of the nuclear lifetime distribution can be obtained through the reduced neutron width, which provides valuable information independent of energy considerations.

The neutron scattering reaction encompasses only one decay channel ($\nu = 1$). Owing to the extreme complexity and random nature of the initial state [36], the neutron width Γ_n follows a zero-mean normal distribution. Therefore, the reduced neutron width Γ_n^0 conforms to the Porter-Thomas ($P-T$) distribution, which can be expressed as [37]

$$P_{PT}(x)\mathrm{d}x = \frac{1}{\sqrt{2\pi c}} e^{-\frac{x}{2}dx}. \tag{11}$$

where $x = \Gamma_n^0/\langle\Gamma_n^0\rangle$ denotes the fluctuation in the normalized reduced width. However, it is typical for comparisons between the experimental data and the expected $P-T$ distribution to be articulated in terms of the integral of the $P-T$ distribution, interpreted as a function of x_i

$$N(x_i) = N_0 \int_{x_i}^{\infty} P_{PT}(x)\mathrm{d}x = N_0\Big(1 - erf\sqrt{x_i/2}\Big). \tag{12}$$

where N_0 is the total number of resonances.

In the present work, the distribution of neutron widths was only studied between 1 eV and 100 eV because of the lack of resonances. Figure 5 illustrates the experimentally observed and computationally derived resonance numbers with $\Gamma_n^0 > x_i\langle\Gamma_n^0\rangle$ as functions of x_i. Hence, our experimental data exhibit remarkably good agreement with the expected $J = 1$-resonance behavior. This result substantiates the consistency of the resonance parameters within the energy range with the least resonance overlap.

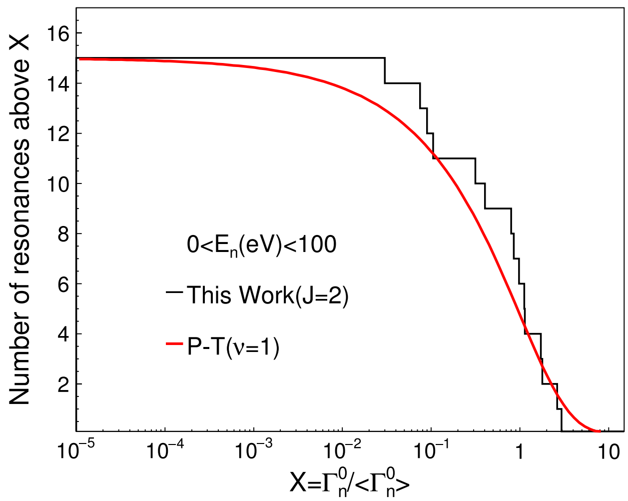

Fig. 5 (Color online) Comparison between the experimental and expected integral distributions of the neutron widths

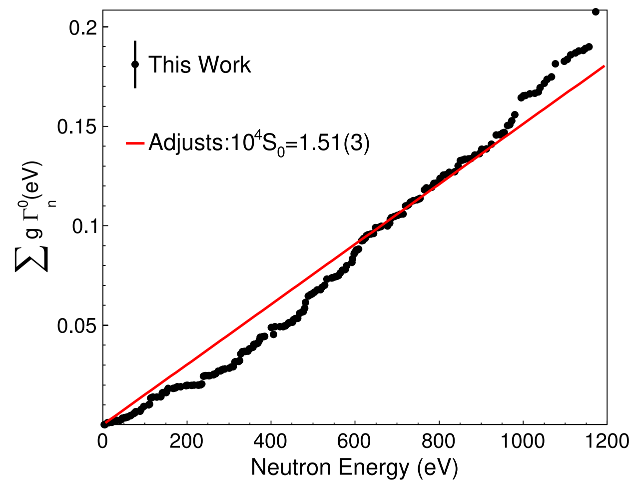

Fig. 6 (Color online) Cumulative sum of the reduced neutron widths as a function of neutron energy

3.3 Neutron strength function

In optical models [38], the neutron strength function S_0, radiation width $\langle\Gamma_\gamma\rangle$, and average level spacing $\langle D\rangle$ are crucial for determining high-energy neutron cross sections. The ratio of the average level spacing to the spacing between the resonances is the neutron strength function or S_0. This function is associated with the average total cross section. The neutron strength function can be expressed as shown in Eq.(13) for the s-wave neutron because of the good agreement between the experimentally reduced neutron widths and the level spacing with the theoretical P-T distribution and Wigner-Dyson distributions.

$$S_0 = \frac{\langle g\Gamma_n^0\rangle}{\langle D_0\rangle} = \frac{\sum_E^{E+\Delta E} g\Gamma_n^0}{\Delta E}, \tag{13}$$

where g is the statistical spin factor. This implies that the neutron strength function can be calculated based on the slope of the cumulative distribution of $g\Gamma_n^0$, which represents the neutron energy. The uncertainty of the strength function is expressed as

$$\frac{\Delta S_0}{S_0} = \sqrt{\frac{1}{N}\left(\frac{4}{\pi}+1\right)}. \tag{14}$$

S_0 is derived from a linear fit (red line) to the experimental data (black dots) in the region 1 eV – 1.2 keV, as shown in Fig. 6. Comparisons of the present S_0 with the literature data are presented in Table 1. Early neutron capture experiments on ^{159}Tb had experimental limitations, resulting in the determination of neutron strength functions ranging from 0.9×10^{-4} to 1.56×10^{-4} within a restricted energy range. The current S_0 value is more reliable for applications due to improved detector performance and a wider neutron energy range in the experiment. The average resonance parameters obtained from this study and in the literature are shown in Table 2.

4 Average resonance cross section

In the URR, the resonances start to overlap as the excitation energy of the compound nuclei increases. While the resonance structures are still visible, their overlap becomes too large to allow for a good match because the intrinsic widths are close to the distance between the neutron cross sections of neighboring resonances.

Table 1 The neutron strength function in different experiments

E_n (eV)	Year	Authors & references	S_0 ($\times10^{-4}$)
3.34–1200	2023	This work	1.51 ± 0.03
Below 1200	1979	Ohkubo [9]	1.55 ± 0.15
Below 580	1979	Ohkubo [9]	1.38 ± 0.18
2590–3464	1978	Mizumoto [6]	1.56
21.2–580	1977	Popov [39]	1.25 ± 0.17
21.2–753	1976	Derrien [40]	1.56 ± 0.02
3.34–97.5	1964	Wang [8]	0.90 ± 0.30
3.34–156	1955	Harvey [35]	1.50 ± 0.20

Therefore, analyzing average cross sections in the URR is more appropriate than analyzing indirect quantities like capture or transmission yields. The relationship between the average neutron capture yield $\langle Y(E_n)\rangle$, average cross section $\langle \sigma_\gamma(E_n)\rangle$, and target thickness n can be represented by the following equation:

$$\langle Y(E_n)\rangle = f(E_n) n \langle \sigma_\gamma(E_n)\rangle. \tag{15}$$

where $f(E_n)$ is the correction factor for the multiple scattering and self-shielding of a target of thickness n.

Currently, SAMMY cannot implement multiple scattering corrections in the URR. Self-shielding and multiple scattering effects are accounted for by $f(E_n)$ factors, which are computed using the SESH code, which is a Monte Carlo code that takes nuclear properties, resonance parameters, and sample geometry specifications as inputs [41]. It then uses these values to generate an average cross section via the Hauser-Feshbach equation and subsequently calculates the average number of collisions before incident neutron capture (or escape). After fitting the SESH data using the function a/E^b, the magnitude of the correction was found to be less than the expected 1% over the entire energy range, as shown in Fig. 7. Therefore, after subtracting the point-by-point background using Eq. (15), the average capture cross section was calculated directly from the capture yield. Because the normalization of capture yields was shown to be accurate and consistent in RRR, the same normalization was applied in URR.

The SAMMY code incorporates Fröhne's FITACS with minor modifications [42]. FITACS uses the Hauser-Feshbach theory with width fluctuations, each partial wave has adjustable parameters for the neutron strength function S_l, the level spacing $\langle D\rangle$, the average radiation width $\langle \Gamma_\gamma\rangle$, and the long-range level parameter R^∞ from the potential scattering radius R_0, where $R_0 = a \cdot (1 - R^\infty)$ and a is the nuclear radius given by $a = 1.23A^{1/3} + 0.8$ fm. These quantities can easily be determined by fitting the experimental neutron capture yield to the initial values determined in RRR. In this study, the FITACS code was used to analyze the contributions of different partial waves to the average cross sections. In FITACS, the level-information data for commonly used inelastic channels are obtained from the ENSDF [43] or JEFF−3.3 [11] databases. The contributions of the first three partial waves were sufficient up to 1 MeV. In the fitting process, the initial values of the resonance parameters were adopted from the present results of the RRR analysis of the s-wave and the data of Mughabghab [34] for the p- and d-waves, respectively.

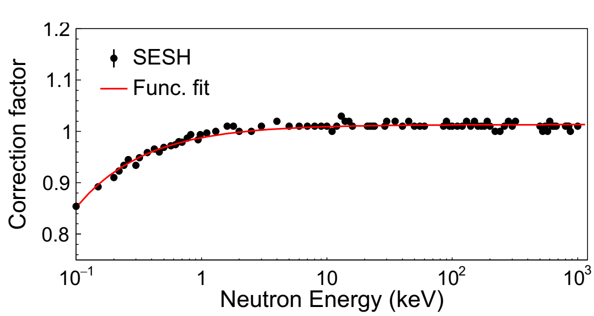

Fig. 7 (Color online) Correction factor for multiple scattering and self-shielding calculated with the SESH code

The FITACS-calculated average cross section and contributions from the first three partial waves ($l = 0, 1, 2$) are shown in Fig. 8. The fitted values obtained from the FITACS code were $S_0 = 1.51(3) \times 10^{-4}$, $S_1 = 1.83(5) \times 10^{-4}$, and $S_2 = 1.55(21) \times 10^{-4}$ [13]. A comparison of various average resonance parameters used to describe URR is presented in Table 3. The calculations indicate that the cross section below 50 keV is dominated by the s-wave. Between 50 and 300 keV, the s-wave and p-wave contributions are comparable, while the d-wave contribution starts to appear above 100 keV. The importance of the p

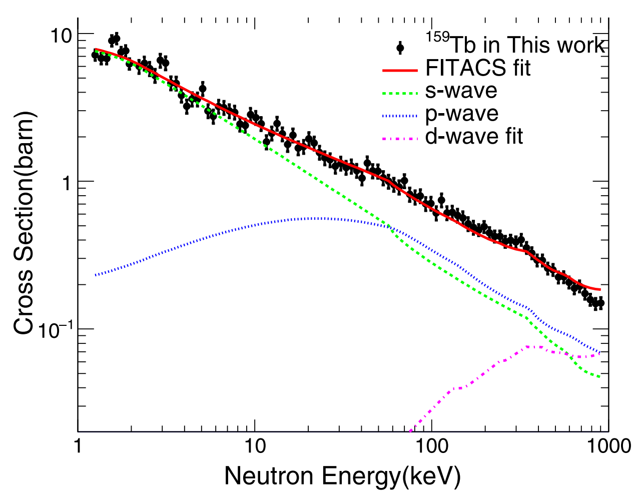

Fig. 8 (Color online) The measured ^{159}Tb capture cross sections and the FITACS code calculation results. The black dots are the measured results from this work; the red solid line is the calculation result from the FITACS code. The green, blue, and pink lines represent the relative contributions of the s-wave, p-wave, and d-wave neutrons ($l = 0$, 1, 2), respectively

Table 2 Average resonance parameters obtained in this study and in the literature

		D_0 (eV)	S_0 ($\times 10^{-4}$)	Γ_γ (meV)
This Work	2023	3.84(4)	1.51(3)	102.6(13)
Muhabghab	2018 [34]	3.84(16)	1.55 (15)	101(2)
Ohkubo	1978 [9]	4.4	1.55(15)	107(7)
Mizumoto	1978 [6]	3.21(1)	1.56	97
ENDF/B-VIII.0	2018 [7]	3.21	1.207	97(7.5)

-wave effect is evident at energies as low as a few keV. The quenching above 50 keV is likely due to competition from inelastic scattering processes, which become significant at higher energies.

5 Summary and conclusion

The neutron capture yield for ^{159}Tb was measured using at the CSNS Back-n facility with an energy detection system (C_6D_6) from 1 electron volt to 1 M electron volt . The resonance parameters for ^{159}Tb were analyzed using the multilevel *R*-matrix Bayesian code SAMMY between 1 eV and 1.2 keV and used for statistical analysis to determine the average quantities required for the cross-section model calculations. The average reduced neutron widths Γ_n^0 and average level spacing D_0 for ^{159}Tb were well fitted by the theoretical Porter-Thomas and Wigner distributions, respectively. The average radiation width $\langle\Gamma_\gamma\rangle$ was calculated to be 102.6(13) meV. The s-wave neutron strength function S_0 derived from Γ_n^0 and D_0 was $1.51(3) \times 10^{-4}$. Statistical analysis of the average capture cross section in the URR was performed using the FITACS code as the input of the RRR average resonance parameters. The results show that the dominant contribution to the cross section comes from the *s*-wave over the entire energy range. The contributions of the *s*- and *p*-waves should also be considered above 50 and 300 keV, respectively. The present work may provide guidance for the reevaluation of the updated nuclear data library and the improvement of nuclear theoretical models.

Appendix A Resonance parameters

The resonance parameters were obtained by fitting the measured capture yield of ^{159}Tb(n, γ) using the *R*-matrix code SAMMY. See Table 3.

Author Contributions All authors contributed to the study conception and design. Material preparation, data collection and analysis were performed by De-Xin Wang, Su-Ya-La-Tu Zhang, Wei Jiang, Jie Ren,

Table 3 Resonance parameters up to 100 eV neutron energy for ^{159}Tb(n, γ) reaction

E_R (eV)	J	l	This work		JEFF−3.3	
			Γ_n (meV)	Γ_γ (meV)	Γ_n (meV)	Γ_γ (meV)
3.34 ± 0.03	2	0	0.34 ± 0.02	102.12 ± 0.06	0.34	103.00
4.97 ± 0.13	1	0	0.07 ± 0.05	100.58 ± 0.04	0.08	103.00
11.04 ± 0.03	2	0	4.97 ± 0.15	105.45 ± 0.02	7.69	99.00
14.40 ± 0.30	2	0	0.12 ± 0.04	98.36 ± 0.08	0.19	105.00
21.19 ± 0.13	1	0	1.23 ± 0.15	103.15 ± 0.23	1.14	102.00
24.53 ± 0.07	2	0	3.77 ± 0.16	128.35 ± 1.40	5.32	116.00
27.55 ± 0.34	2	0	0.48 ± 0.09	95.68 ± 0.85	0.83	102.00
33.83 ± 0.12	1	0	3.24 ± 0.52	102.32 ± 0.48	2.61	98.00
40.81 ± 0.63	1	0	0.55 ± 0.18	105.78 ± 1.73	0.84	101.00
43.69 ± 0.13	2	0	4.33 ± 0.28	103.54 ± 1.25	5.90	97.00
46.04 ± 0.14	2	0	7.62 ± 0.52	113.48 ± 1.29	13.94	109.00
50.16 ± 0.24	2	0	1.80 ± 0.12	102.86 ± 0.61	1.91	96.00
51.61 ± 0.38	1	0	1.14 ± 0.21	98.36 ± 1.43	0.84	96.00
54.08 ± 0.53	2	0	0.41 ± 0.16	85.51 ± 1.23	0.83	78.00
57.45 ± 0.36	1	0	2.09 ± 0.38	102.48 ± 1.00	2.20	99.00
58.77 ± 0.29	2	0	1.38 ± 0.22	98.65 ± 0.79	1.59	96.00
65.17 ± 0.18	2	0	7.90 ± 0.54	98.25 ± 1.44	12.61	96.00
66.56 ± 0.39	1	0	1.82 ± 0.51	93.22 ± 1.10	3.52	98.00
73.83 ± 0.14	2	0	14.31 ± 0.82	102.34 ± 1.28	19.09	98.00
76.45 ± 0.29	1	0	7.35 ± 0.98	116.67 ± 2.79	6.92	108.00
77.98 ± 0.37	2	0	4.85 ± 0.92	101.13 ± 2.56	7.25	96.00
78.80 ± 0.67	2	0	1.06 ± 0.62	95.15 ± 2.00	2.68	85.00
88.44 ± 0.42	2	0	3.54 ± 0.66	86.62 ± 1.11	3.37	70.00
90.60 ± 0.33	2	0	11.72 ± 1.75	105.68 ± 2.74	6.84	90.00
97.24 ± 0.31	1	0	24.37 ± 5.12	118.76 ± 4.77	38.21	101.00

Mei-Rong Huang, Jing-Yu Tang, Xi-Chao Ruan, Hong-Wei Wang, Long-Xiang Liu, Xue Li, Dan-Dan Niu, Guo Li, Gu-Fu Meng, Yong-Shun Huang, Zhi-Long Wang, Yu Bai and Xue Yang. The first draft of the manuscript was written by De-Xin Wang. All authors commented on previous versions of the manuscript. All authors read and approved the final manuscript.

Data Availability The data that support the findings of this study are openly available in Science Data Bank at https://cstr.cn/31253.11.sciencedb.16674 and https://www.doi.org/10.57760/sciencedb.16674.

Declarations

Conflict of interest The authors declare that they have no conflict of interest.

References

1. S.I. Sukhoruchkin, Z.N. Soroko, in *Neutron Resonance Parameters*, ed. by H. Schopper (Springer, Berlin Heidelberg New York, 2015) Supplement to Volume I/24, p. 2181. https://doi.org/10.1007/978-3-662-45603-3
2. Z.Y. Bao, F. Käppeler, Neutron capture cross sections for s-process studies. At. Data Nucl. Data Tables **36**, 411 (1987). https://doi.org/10.1016/0092-640X(87)90011-8
3. G. Noguere, O. Bouland, J. Heyse et al., *s*-wave average neutron resonance parameters of ^{175}Lu+n. Phys. Rev. C **100**, 065806 (2019). https://doi.org/10.1103/PhysRevC.100.065806
4. K.K. Seth, S-wave neutron strength functions. Nucl. Data Sheets. Sects. A **2**, 299 (1966). https://doi.org/10.1016/S0550-306X(66)80008-3
5. V.V. Zerkin, B. Pritychenko, The experimental nuclear reaction data (EXFOR): extended computer database and Web retrieval system. Nucl. Instrum. Methods. A **888**, 31 (2018). https://doi.org/10.1016/j.nima.2018.01.045
6. M. Mizumoto, R.L. Macklin, J. Halperin, Neutron capture cross section of ^{159}Tb from 2.6 to 700 keV. Phys. Rev.C **17**, 522 (1978) https://doi.org/10.1103/PhysRevC.17.522
7. D. A. Brown, M. B. Chadwick, R. Capote *et al.*, ENDF/B-VIII.0: the 8th major release of the nuclear reaction data library with CIELO-project cross sections, new standards and thermal scattering data. Nucl. Data Sheets **148**,1 (2018). https://doi.org/10.1016/j.nds.2018.02.001
8. N.Y. Wang, N. Iliescu, E.N. Karzhavina et al., Neutron resonances in praseodymium and terbium. Soviet Phys. J. Exptl. Theoret. Phys. **47**, 43 (1964)
9. M. Ohkubo, Y. Kawarasaki, Slow neutron resonances in terbium-159. J. Nucl. Sci. Technol. **16**, 10 (1979). https://doi.org/10.1080/18811248.1979.9730969
10. S.F. Mughabghab, in*Atlas of Nntron Cross Section, Vol. I, Part B*, 3th edn. (Academic Press, New York, 1984), pp.121-128
11. A.J.M. Plompen, O. Cabellos, C. De Saint Jean *et al.*, The joint evaluated the fission and fusion nuclear data library JEFF-3.3. Eur. Phys. J. A **56**, 181 (2020). https://doi.org/10.1140/epja/s10050-020-00141-9
12. J.Y. Tang, Q. An, J.B. Bai et al., A back-n white-neutron source at CSNS and its applications. Nucl. Sci. Tech. **32**, 1 (2021). https://doi.org/10.1007/s41365-021-00846-6
13. S. Zhang, G. Li, W. Jiang et al., Measurement of the ^{159}Tb(n, γ) cross-section at the CSNS Back-n facility. Phys. Rev. C **107**, 045809 (2023). https://doi.org/10.1103/PhysRevC.107.045809
14. J.Y. Tang, R. Liu, G.H. Zhang et al., Initial years' neutron-induced cross-section measurements at the CSNS Back-n white neutron source. Chin. Phys. C **45**, 062001 (2021). https://doi.org/10.1088/1674-1137/abf138
15. J. Ren, X.C. Ruan, W. Jiang et al., Background study of (n, γ) cross-sectional measurements with C_6D_6 detectors at CSNS Back-n. Nucl. Instr. and Meth. A **985**, 164703 (2021). https://doi.org/10.1016/j.nima.2020.164703
16. Y.H. Chen, G.Y. Luan, J. Bao et al., Neutron energy spectrum measurement of back-n white neutron source at CSNS. Eur. Phys. J. A **55**, 1 (2019). https://doi.org/10.1140/epja/i2019-12808-1
17. X.X. Li, L.X. Liu, W. Jiang et al., New experimental measurement of ^{nat}Er(n, γ) cross-sections between 1 and 100 eV. Phys. Rev. C **104**, 054302 (2021). https://doi.org/10.1103/PhysRevC.104.054302
18. X.R. Hu, G.T. Fan, W. Jiang et al., Measurements ofthe ^{197}Au(n, γ) cross-section up to 100 keV at the CSNS Back-nfacility. Nucl. Sci. Tech. **32**, 1 (2021). https://doi.org/10.1007/s41365-021-00931-w
19. X.X. Li, L.X. Liu, W. Jiang et al., The experimental determination of the neutron resonance peak of ^{162}Er at 67.8 eV. Phys. Rev. C **106**, 065804 (2022). https://doi.org/10.1103/PhysRevC.106.065804
20. D.X. Wang, S. Zhang, W. Jiang et al., Neutron capture cross-sectional measurements for ^{nat}Lu with different thicknesses. Acta. Phys. Sin. **71**, 072901 (2022). https://doi.org/10.7498/aps.71.20212051
21. J. Ren, X.C. Ruan, W. Jiang et al., The neutron capture cross-section of ^{169}Tm measured at the CSNS Back-n facility in the energy region from 30 to 300 keV. Chin. Phys. C **46**, 044002 (2022). https://doi.org/10.1088/1674-1137/ac4589
22. G.L. Yang, Z.D. An, W. Jiang et al., Measurement of Br(n,γ) cross-sections up to stellar s-process temperatures at CSNS Back-n. Nucl. Sci. Tech. **34**, 180 (2023). https://doi.org/10.1007/s41365-023-01337-6
23. G.L. Yang, Z.D. An, W. Jiang et al., Measurement of neutron capture cross sections of rhenium up to stellar s-and r-process temperatures at the China Spallation Neutron Source Back-n facility. Phys. Research **6**, 013225 (2024). https://doi.org/10.1103/PhysRevResearch.6.013225
24. J.M. Xue, S. Feng, Y.H. Chen et al., Measurement of the neutron-induced total cross sections of ^{nat}Pb from 0.3 eV to 20 MeV on the Back-n at CSNS. Nucl. Sci. Tech. **35**, 18 (2024). https://doi.org/10.1007/s41365-024-01370-z
25. J.C. Wang, J. Ren, W. Jiang et al., The in-beam gamma rays of CSNS Back-n are characterized by a black resonance filter. Nucl. Sci. Tech. **35**, 164 (2024). https://doi.org/10.1007/s41365-024-01553-8
26. X. K. L, Z. D. An, W. Jiang *et al.*, Measurement of the ^{141}Pr(n,γ) cross section up to stellar s-process temperatures at the China spallation neutron source Back-n facility, Phys. Rev. C **108**, 035802 (2023). https://doi.org/10.1103/PhysRevC.108.035802
27. S. Agostinelli, J. Allison, K. Amako et al., GEANT4-a simulation toolkit. Nucl. Instr. Meth. A. **506**, 250 (2003). https://doi.org/10.1016/S0168-9002(03)01368-8
28. R.L. Macklin, J.H. Gibbons, Capture cross-sectional studies for 30–220-keV neutrons using a new technique. Phys. Rev. **159**, 4 (1967). https://doi.org/10.1103/PhysRev.159.1007
29. N. M. Larson, *Updated users guide for SAMMY: multilevel The R-matrix fits the neutron data using Bayes equations. No. ORNL/TM- 2809179/R8* (Oak Ridge Naional Laboratory 2008)
30. S. Amaducci, N. Colonna, L. Cosentino et al., Measurement of the ^{140}Ce(n, γ) cross section at *n*_TOF and its astrophysical implications for the chemical evolution of the universe. Phys. Rev. Lett. **132**, 122701 (2024). https://doi.org/10.1103/PhysRevLett.132.122701

31. C. Lederer-Woods, J. Andrzejewski, U. Battino et al., Measurement of the ^{70}Ge(n, γ) cross-section up to 300 keV at the CERN nTOF facility. Phys. Rev. C **100**, 045804 (2019). https://doi.org/10.1103/PhysRevC.100.045804
32. V.P. Alfimenkov, S.B. Borzakov, J. Wierzbicki et al., Investigation of the spin dependence of neutron cross sections and strength functions for rare earth nuclei in experiments with polarized neutrons and nuclei. Nucl. Phys. A **376**, 2 (1982). https://doi.org/10.1016/0375-9474(82)90062-87
33. E.P. Wigner, *Conference on Neutron Physics by Time of Flight (Gatlinburg, Tennessee, November 1956), Report ORNL-2309* (Oak Ridge Naional Laboratory, 1957)
34. S. F. Mughabghab, *Atlas of Neutron Resonances*, 6th edn. (Elsevier, Amsterdam, 2018), pp.178 https://doi.org/10.1016/B978-0-44-463780-2.00015-3
35. J.A. Harvey, D.J. Hughes, R.S. Carter et al., Spacing and neutron widths of nuclear energy levels. Phys. Rev. **99**, 10 (1955). https://doi.org/10.1103/PhysRev.99.10
36. C.E. Porter, N. Rosenzweig, Repulsion of energy levels in complex atomic spectra. Phys. Rev. **120**, 1698 (1960). https://doi.org/10.1103/PhysRev.120.1698
37. C.E. Porter, R.G. Thomas, Fluctuations in the nuclear reaction widths. Phys. Rev. **104**, 483 (1956). https://doi.org/10.1103/PhysRev.104.483
38. L.C. Gomes, Imaginary part of the optical potential. Phys. Rev. **116**, 1226 (1959). https://doi.org/10.1103/PhysRev.116.1226
39. A.B. Popov, H. Faikov et al., Yad. Fiz **26**, 14 (1977)
40. J. Blons, H. Derrien, Analyse multiniveaux des sections efficaces totale et de fission de ^{241}Pu de 1 à 104 eV. J. Phys. France **37**, 6 (1976). https://doi.org/10.1051/jphys:01976003706065900
41. F.H. Frohner., SESH Computer Code. Gulf General Atomic Report, GA-8330 (1968)
42. F.H. Frohner., FITACS computer code. Rep. ANL-83-4 (1983)
43. M. R. Bha. *Nuclear Data for Science and Technology*, ed. by s. m. Qaim, (Springer, Berlin Heidelberg New York, 1992), p. 1 https://doi.org/10.1007/978-3-642-58113-7-227